A Linear Height-Resolving Wind Field Model for Tropical Cyclone Boundary Layer

Reda Snaiki, Teng Wu*

Department of Civil, Structural and Environmental Engineering, University at Buffalo, State University of New York, Buffalo, NY 14126, USA

*Corresponding author. Email: tengwu@buffalo.edu

Abstract: The wind field model is one of the most important components for the tropical cyclone hazard assessment, thus the appropriate design of this element is extremely important. While solving the fully non-linear governing equations of the wind field was demonstrated to be quite challenging, the linear models showed great promise delivering a simple solution with good approximation to the wind field, and can be readily adopted for engineering applications. For instance it can be implemented in the Monte Carlo technique for rapid tropical-cyclone risk assessment. This study aims to develop a height-resolving, linear analytical model of the boundary layer winds in a moving tropical cyclone. The wind velocity is expressed as the summation of two components, namely gradient wind in the free atmosphere and frictional component near the ground surface. The gradient wind was derived straightforwardly, while the frictional component was obtained based on the scale analysis of the fully non-linear Navier-Stokes equations. The variation of wind field with respect to the angular coordinate was highlighted since its contribution to the surface wind speed and associated spatial distribution cannot be ignored in the first-order approximation. The results generated by the present model are consistent with tropical cyclone observations.

Key words: Height-resolving wind-field model, Boundary layer, Scale analysis, Tropical cyclone.

1. Introduction

Tropical cyclone-related natural hazards are well known for resulting in the largest contribution to insured losses each year. High winds in the tropical cyclone boundary layer cause widespread damage to life and property in coastal areas. This situation has become more challenging due to the changing climate and increasing coastal population density. A mature tropical cyclone typically consists of four dynamically distinct parts, namely a boundary layer, a region above the boundary layer (almost no radial motion), an updraft region, and a quiescent eye (Carrier et al. 1971). For many engineering applications, only the boundary layer is concerned. Furthermore, in the consideration of wind-induced damages, the dynamics of boundary layer, where the density changes could be ignored, and the thermodynamics are usually independently examined, or weakly coupled.

The dynamics of tropical cyclone boundary layer is essentially governed by the Navier-Stokes equations of incompressible flow. The solution of dynamically coupled, intensively interactive pressure and velocity fields is extremely challenging. In most of wind field models for engineering applications, the pressure field (steady pressure gradient) is usually prescribed, either based on the gradient wind equation (e.g., Shapiro 1983) or resulting from an empirical formula (e.g., Schloemer 1954; Holland 1980). The wind speed could be simulated based on a slab (depth-averaged) or height-resolving model. The slab wind field model has been widely applied to storm surge modeling (e.g., Hubbert et al. 1991; Kennedy et al. 2012) and hurricane damage and loss estimation (e.g., Florida Hurricane Loss Projection Model and HAZUS-MH Hurricane Model) (Powell et al. 2005; Vickery et al. 2006) since the pioneering work of Chow (1971), Shapiro (1983), and Thompson and Cardone (1996). However, there are several inherent limitations of the slab model due to the vertical averaging of dynamic quantities in the boundary layer, as comprehensively discussed by several studies (e.g., Kepert 2010a; 2010b). Among a series of shortcomings, considering the boundary layer height as a constant and obtaining the near surface winds based on empirical-based reduction factors may have considerable impact on the simulation fidelity. Recently, Khare et al. (2009) has shown the linear height-resolving model is superior to the slab model of tropical cyclone boundary layer based on the observation data of over-ocean surface wind field.

The height-resolving model was originally derived by studying the tropical cyclone boundary layer as a generalized Ekman problem (Haurwitz 1935; 1936; Rosenthal 1962). Later, Yoshizumi (1968) integrated the storm movement into the model to account for the left-right asymmetry of tropical cyclone wind field. On the other hand, Meng (1995; 1997) obtained similar height-resolving solutions of boundary layer winds by carrying out perturbation analysis of the Navier-Stokes equations. A so-called equivalent roughness length was introduced in Meng's model (1995; 1997) to simultaneously take the terrain roughness and topographical effects into account, whereas the estimation of the equivalent roughness length for each case is not straightforward. It should be noted that the abovementioned height-resolving models are actually linear solutions. The state-of-the-art tropical cyclone risk assessment is essentially based on the analysis framework established by Russell (1971), where the Monte Carlo sampling method is utilized. This indicates a large number of simulations of the tropical cyclone boundary layer wind filed are usually needed. Although nonlinear effects may not be always insignificant especially for local flows (Kepert 2001; Kepert and Wang 2001), it is believed that the linear height-resolving wind field model is a reasonable choice for many engineering applications (including risk assessment) due to its high simulation efficiency.

In this study, the linear height-resolving wind field model was extracted based on the scale analysis of the Navier-Stokes equations. The analytical expressions for wind speed components of the tropical cyclone boundary layer were derived since they could facilitate the interpretation of underlying physics. The obtained linear governing equations for boundary layer wind field are different from those of previously widely-discussed models (Meng et al. 1995; Kepert 2001). For example, several new terms that account for the contributions from the azimuthal variation of velocity components are retained. It was demonstrated that the modification of surface wind speed and its spatial distribution resulting from these new terms cannot be ignored. The new linear height-resolving wind field model was validated using the observation data obtained during a typhoon and a hurricane, respectively. Compared with Meng's simulation, the new proposed model shows improved representation of the wind field in the tropical cyclone boundary layer.

2. Boundary Layer Wind Model

In the boundary layer of a tropical cyclone, the horizontal momentum equations are typically solved with a prescribed pressure distribution and a constant air density. Thus, the governing equation of the wind field of a tropical cyclone is:

$$\frac{\partial \boldsymbol{v}}{\partial t} + \boldsymbol{v}.\nabla \boldsymbol{v} = -\frac{1}{\rho}\nabla p - f\boldsymbol{k} \times \boldsymbol{v} + \boldsymbol{F} \tag{1}$$

where $\boldsymbol{v}$ = wind velocity; t= time; f = Coriolis parameter; $\boldsymbol{k}$ = unit vector in the vertical direction; ρ = air density; $\boldsymbol{F}$ = frictional force; and p = Holland pressure expressed as:

$$p = p_c + \Delta p \exp\left[-\left(r_m / r\right)^B\right] \tag{2}$$

where p_c = central pressure; Δp = central pressure difference; r_m = radius of maximum winds; r = radial distance from the tropical cyclone center; and B = Holland's radial pressure parameter. It should be noted that bold character denote a vector. Eq. (1) is supplemented by the continuity equation:

$$\frac{d\rho}{dt} = -\rho\nabla.\boldsymbol{v} \tag{3}$$

which becomes for an incompressible flow:

$$\nabla.\boldsymbol{v} = 0 \tag{4}$$

To solve the governing equation of motion, the wind velocity ($\boldsymbol{v}$) is expressed as the summation of the gradient wind in the free atmosphere ($\boldsymbol{v}_g$) and the frictional component near the ground surface ($\boldsymbol{v}'$):

$$\boldsymbol{v} = \boldsymbol{v}_g + \boldsymbol{v}' \tag{5}$$

Consequently two separate equations can be derived:

$$\frac{\partial \boldsymbol{v}_g}{\partial t} + \boldsymbol{v}_g.\nabla\boldsymbol{v}_g = -\frac{1}{\rho}\nabla p - f\boldsymbol{k}\times\boldsymbol{v}_g \tag{6a}$$

$$\frac{\partial \boldsymbol{v}'}{\partial t} + \boldsymbol{v}'.\nabla\boldsymbol{v}' + \boldsymbol{v}'.\nabla\boldsymbol{v}_g + \boldsymbol{v}_g.\nabla\boldsymbol{v}' = -f\boldsymbol{k}\times\boldsymbol{v}' + \boldsymbol{F} \tag{6b}$$

Similar to Meng et al. (1995), the gradient wind pattern $\boldsymbol{v}_g$ is assumed to move in the free atmosphere, at the translation velocity of the tropical cyclone $\boldsymbol{c}$, thus the unsteady term can be expressed as: $\frac{\partial \boldsymbol{v}_g}{\partial t} = -\boldsymbol{c}.\nabla\boldsymbol{v}_g$. On the other hand, the unsteady term $\frac{\partial \boldsymbol{v}'}{\partial t}$ is significantly smaller than the turbulent viscosity and inertia terms in the tropical cyclone boundary layer, and hence neglected.

2.1 Gradient wind velocity

The cylindrical coordinate system (r, θ, z) whose origin is located at the center of the tropical cyclone is used to solve the governing equations. Fig. 1 illustrates the necessary parameters needed for the present study, where υ= approach angle (counterclockwise positive from the East); θ= azimuthal angle (counterclockwise positive from the East); h = mean height of the roughness elements; $z_{10} = 10m$ height above the mean height of roughness elements; and z'= new vertical coordinate used as the base of the computation scheme where $z' = 0$ is located at $h + z_{10}$.

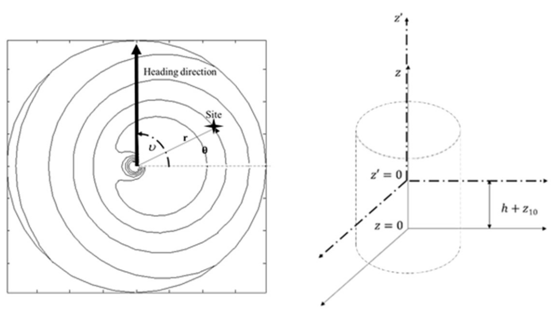

Fig. 1. Cylindrical coordinate system

Accordingly, Eq. (6a) could be expressed as:

$$\left(v_{rg} - c.\cos\left(\theta - \upsilon\right)\right)\frac{\partial v_{rg}}{\partial r} + \frac{v_{\theta g} + c.\sin\left(\theta - \upsilon\right)}{r}\frac{\partial v_{rg}}{\partial \theta} - \frac{{v_{\theta g}}^{2}}{r} - \frac{v_{\theta g} c.sin\left(\theta - \upsilon\right)}{r} = -\frac{1}{\rho}\frac{\partial p}{\partial r} + f v_{\theta g} \tag{7a}$$

$$\left(v_{rg} - c.cos\left(\theta - \upsilon\right)\right)\frac{\partial v_{\theta g}}{\partial r} + \frac{v_{\theta g} + c.\sin\left(\theta - \upsilon\right)}{r}\frac{\partial v_{\theta g}}{\partial \theta} + \frac{v_{\theta g} v_{rg}}{r} + \frac{v_{rg} c.\sin\left(\theta - \upsilon\right)}{r} = -f v_{rg} \tag{7b}$$

The radial velocity v_{rg} could be derived based on the continuity equation, which, due to its insignificant effect, is usually disregarded as suggested by Meng et al. (1995). Hence, $v_{\theta g}$ could be derived from Eq. (7a) as:

$$v_{\theta g} = \frac{\left(-c\sin(\theta-\upsilon)-fr\right)}{2} + \left[\frac{\left(-c\sin(\theta-\upsilon)-fr\right)^2}{4} + \frac{r}{\rho}\frac{\partial p}{\partial r}\right]^{1/2} \tag{8}$$

The solution of gradient wind velocity is straightforward and was discussed in detail by several researchers (e.g. Georgiou 1986; Meng et al. 1995).

2.2 Frictional wind velocity

The absolute angular velocity and vertical component of absolute vorticity of the gradient wind are introduced first and given respectively by the following formulas (Meng et al. 1995):

$$\xi_g = \frac{2v_{\theta g}}{r} + f \tag{9a}$$

$$\xi_{ag} = \frac{\partial v_{\theta g}}{\partial r} + \frac{v_{\theta g}}{r} + f \tag{9b}$$

As a result, Eq. (6b) in the cylindrical coordinate becomes:

$$u'\frac{\partial u'}{\partial r} + \frac{v_{\theta g}+v'}{r}\frac{\partial u'}{\partial \theta} + w\frac{\partial u'}{\partial z} - \frac{v'^2}{r} - \xi_g v' = K\left[\nabla^2 u - \frac{1}{r^2}\left(u + 2\frac{\partial v}{\partial \theta}\right)\right] \tag{10a}$$

$$u'\frac{\partial v'}{\partial r} + \frac{v_{\theta g}+v'}{r}\frac{\partial v'}{\partial \theta} + w\frac{\partial v'}{\partial z} + \frac{u'v'}{r} + \xi_{ag} u' + \frac{v'}{r}\frac{\partial v_{\theta g}}{\partial \theta} = K\left[\nabla^2 v - \frac{1}{r^2}\left(v - 2\frac{\partial u}{\partial \theta}\right)\right] \tag{10b}$$

where (u,v,w) = velocity vector; and u', v' are the frictional components of the wind velocity. The right hand side of Eqs. (10a) and (10b) represents the radial and azimuthal frictional force components, respectively. The turbulent diffusivity K is assumed to be constant in this study.

The continuity equation can be expressed in the cylindrical coordinates as:

$$\frac{1}{r}\frac{\partial(ru)}{\partial r} + \frac{1}{r}\frac{\partial v}{\partial \theta} + \frac{\partial w}{\partial z} = 0 \tag{11}$$

Then the vertical component of the wind velocity can be derived:

$$w = -\frac{1}{r}\frac{\partial}{\partial r}\left(r\int_0^z u dz\right) - \frac{1}{r}\frac{\partial}{\partial \theta}\left(\int_0^z v dz\right) \tag{12}$$

Solving Eqs. (10a) and (10b) analytically is extremely difficult. In this study, they will be first simplified using the scale analysis approach.

2.3 Scale analysis

In this section the same notation used by Vogl and Smith (2009) will be adopted for denoting the scales of various quantities in Eqs. (10a) and (10b), as showed in Table 1:

Table 1. Scales of various quantities

Quantity	u'	v'	$v_{\theta g}$	v	w	r	z	ξ_g	ξ_{ag}	Change in p
Scale	U'	V'	V_g	V	W	R	Z	Ξ	Λ	Δp

Six non-dimensional parameters were introduced in Vogl and Smith (2009), namely Reynolds number $R_e = VZ / K$; local Rossby numbers $Ro_\Lambda = V / (R\Lambda)$ and $Ro_\Xi = V / (R\Xi)$; Swirl parameters $S_{u'} = U' / V$ and $S_{v'} = V' / V$; and $A = Z / R$ that is the aspect ratio of the boundary-layer depth to the radial scale. It should be noted that based on the continuity equation namely Eq. (11), the following result is obtained $U' / R \sim W / Z$.

The scale analysis for Eqs. (10a) and (10b) is presented in Tables 2 and 3, respectively. The non-dimensional form is obtained by multiplying Eqs. (10a) and (10b) by $1 / V'\Xi$ and $1 / U'\Lambda$, respectively. It is worth mentioning that the terms $2\frac{K}{r^2}\frac{\partial u}{\partial \theta}$ and $-2\frac{K}{r^2}\frac{\partial v}{\partial \theta}$ are not included in Tables 2 and 3 since they have the same scale order as $K\left(\nabla_h^2 u - \frac{u}{r^2}\right)$ and $K\left(\nabla_h^2 v - \frac{v}{r^2}\right)$, respectively.

Table 2. Scale analysis of Eq. (10a)

Quantity	Scale	Normalized form
$u'\dfrac{\partial u'}{\partial r}$	U'^2/R	$S_{U'}{}^{2}S_{V'}{}^{-1}Ro_{\Xi}$
$\dfrac{v_{\theta g}+v'}{r}\dfrac{\partial u'}{\partial \theta}$	$\dfrac{(V_g+V')}{R}U'$	$S_{V'}{}^{-1}S_{U'}Ro_{\Xi}$
$w\dfrac{\partial u'}{\partial z}$	WU'/Z	$S_{U'}{}^{2}S_{V'}{}^{-1}Ro_{\Xi}$
$-\dfrac{v'^2}{r}$	V'^2/R	$S_{V'}Ro_{\Xi}$
$-\xi_g v'$	$\Xi V'$	1
$K\left(\nabla_h{}^2 u-\dfrac{u}{r^2}\right)$	KU/R^2	$A\left(R_e S_{V'}\right)^{-1}S_U Ro_{\Xi}$
$K\dfrac{\partial^2 u'}{\partial z^2}$	KU'/Z^2	$\left(AR_e S_{V'}\right)^{-1}S_{U'}Ro_{\Xi}$

Table 3. Scale analysis of Eq. (10b)

Quantity	Scale	Normalized form
$u'\dfrac{\partial v'}{\partial r}$	$U'V'/R$	$S_{V'}Ro_{\Lambda}$
$\dfrac{v_{\theta g}+v'}{r}\dfrac{\partial v'}{\partial \theta}$	$\dfrac{(V_g+V')V'}{R}$	$S_{V'}S_{U'}{}^{-1}Ro_{\Lambda}$
$w\dfrac{\partial v'}{\partial z}$	WV'/Z	$S_{V'}Ro_{\Lambda}$
$\dfrac{u'v'}{r}$	$U'V'/R$	$S_{V'}Ro_{\Lambda}$
$\xi_{ag}u'$	$\Lambda U'$	1
$\dfrac{v'}{r}\dfrac{\partial v_{\theta g}}{\partial \theta}$	$\dfrac{VV'}{R}$	$S_{V'}S_{U'}{}^{-1}Ro_{\Lambda}$
$K\left(\nabla_h{}^2 v-\dfrac{v}{r^2}\right)$	KV/R^2	$A\left(R_e S_{U'}\right)^{-1}Ro_{\Lambda}$
$K\dfrac{\partial^2 v'}{\partial z^2}$	KV'/Z^2	$\left(AR_e S_{U'}\right)^{-1}S_{V'}Ro_{\Lambda}$

Typical values for the boundary layer such as the boundary layer height and the turbulent diffusivity K were considered to assess the magnitude of each term. As a result, a new set of equations could be obtained:

$$u'\frac{\partial u'}{\partial r}+\frac{v_{\theta g}+v'}{r}\frac{\partial u'}{\partial \theta}+w\frac{\partial u'}{\partial z}-\frac{v'^2}{r}-\xi_g v'=K\frac{\partial^2 u'}{\partial z^2} \tag{13a}$$

$$u'\frac{\partial v'}{\partial r}+\frac{v_{\theta g}+v'}{r}\frac{\partial v'}{\partial \theta}+w\frac{\partial v'}{\partial z}+\frac{u'v'}{r}+\xi_{ag}u'+\frac{v'}{r}\frac{\partial v_{\theta g}}{\partial \theta}=K\frac{\partial^2 v'}{\partial z^2} \tag{13b}$$

Solving the above nonlinear equations is demonstrated quite expensive. For engineering purposes, the nonlinear equations could be simplified by linearization techniques.

3. Linear height-resolving model

3.1 Governing equations

Equations (13a) and (13b) could be linearized as:

$$\frac{v_{\theta g}}{r}\frac{\partial u'}{\partial \theta}-\xi_g v'=K\frac{\partial^2 u'}{\partial z^2} \tag{14a}$$

$$\frac{v_{\theta g}}{r}\frac{\partial v'}{\partial \theta}+\xi_{ag}u'+\frac{v'}{r}\frac{\partial v_{\theta g}}{\partial \theta}=K\frac{\partial^2 v'}{\partial z^2} \tag{14b}$$

To solve the above-mentioned governing equations, the boundary conditions at the upper atmosphere (15a) and above the ground surface (15b) need to be respectively employed:

$$\boldsymbol{v}'\big|_{z'\to\infty}=0 \tag{15a}$$

$$\rho K\frac{\partial \boldsymbol{v}'}{\partial z}\bigg|_{z'=0}=\rho C_d\left|\boldsymbol{v}_s\right|\boldsymbol{v}_s \tag{15b}$$

where $\boldsymbol{v}'$ = frictional component of the wind velocity; $\boldsymbol{v}_s$ = total wind velocity near the ground surface; and C_d = drag coefficient.

New variables are introduced to simplify the solution namely: $\alpha=\frac{1}{2K}\xi_g$; $\beta=\frac{1}{2K}\xi_{ag}$; $\gamma=\frac{1}{2K}\frac{v_{\theta g}}{r}$; and $\phi=\frac{1}{2Kr}\frac{\partial v_{\theta g}}{\partial \theta}$. In addition, the variable ω used in Kepert (2001) is employed:

$$\omega = \sqrt{\frac{\beta}{\alpha}} u' + i v' \tag{16}$$

It should be noted that the equations to be solved in this study are different from those in Kepert (2001). Specifically, the equations have an additional term $\frac{v'}{r}\frac{\partial v_{\theta g}}{\partial \theta}$ since the gradient wind velocity is considered to be dependent not only on the radial coordinate but the azimuthal one as well. Furthermore, the translational velocity is integrated into the gradient wind velocity based on the assumption that the wind pattern $\boldsymbol{v_g}$ moves at the translation velocity of the tropical cyclone $\boldsymbol{c}$, while Kepert (2001) assumed a symmetric case of the gradient wind. Finally, the absolute angular velocity ξ_g and vertical component of absolute vorticity of the gradient wind ξ_{ag} are exhibiting not only a radial variation but and azimuthal one as well. Accordingly, Eqs. (14a) and (14b) could be expressed as:

$$2\gamma \frac{\partial \omega}{\partial \theta} + 2i\sqrt{\alpha\beta}\,\omega - \frac{\partial^2 \omega}{\partial z^2} + 2\phi Im(\omega) = 0 \tag{17}$$

$Im(\omega)$ can be written as $i\left(-\omega + \omega^*\right)/2$ (where * indicates a complex conjugate), then Eq. (17) becomes:

$$2\gamma \frac{\partial \omega}{\partial \theta} + i\left(2\sqrt{\alpha\beta} - \phi\right)\omega + \phi i \omega^* - \frac{\partial^2 \omega}{\partial z^2} = 0 \tag{18}$$

The corresponding boundary condition expressed by Eq. (15b) could be decomposed using the cylindrical coordinates into:

$$K\frac{\partial u'}{\partial z} = C_d \sqrt{(u' + v_{rg})^2 + \left(v_{\theta g} + v'\right)^2}\left(v_{rg} + u'\right) \tag{19a}$$

$$K\frac{\partial v'}{\partial z} = C_d \sqrt{(u' + v_{rg})^2 + \left(v_{\theta g} + v'\right)^2}\left(v_{\theta g} + v'\right) \tag{19b}$$

Eqs. (19a) and (19b) can be linearized considering $u',v' \ll v_{\theta g}$, hence, the final system to be solved becomes:

$$2\gamma\frac{\partial\omega}{\partial\theta}+i\left(2\sqrt{\alpha\beta}-\phi\right)\omega+\phi i\omega^{*}-\frac{\partial^{2}\omega}{\partial z^{2}}=0 \tag{20a}$$

$$K.Re\left(\omega'(0)\right)=C_{d}v_{\theta g}\left(v_{rg}+Re\left(\omega(0)\right)\right) \tag{20b}$$

$$K.Im\left(\omega'(0)\right)=C_{d}v_{\theta g}\left(v_{\theta g}+2Im\left(\omega(0)\right)\right) \tag{20c}$$

3.2 Analytical solutions

To solve system (20), ω is expanded as Fourier series in azimuth, i.e., $\omega(\theta,z')=\sum_{k=-\infty}^{\infty}a_{k}(z')e^{ik\theta}$ where $a_{k}(z')$ is a complex coefficient (Kepert 2001). Then Eq. (20a) becomes:

$$\sum_{k=-\infty}^{\infty}\left[i\left(2\gamma k+2\sqrt{\alpha\beta}-\phi\right)a_{k}(z')-a_{k}''(z')+i\phi a_{-k}^{*}(z')\right]e^{ik\theta}=0 \tag{21}$$

The complex coefficient a_k can be expressed as $a_{k}(z')=A_{k}\exp\left(q_{k}z'\right)$, and hence the following equation could be obtained:

$$A_{k}q_{k}^{2}=i\left[2\gamma k+2\sqrt{\alpha\beta}-\phi\right]A_{k}+i\phi A_{-k}^{*} \tag{22}$$

Since the wavenumbers higher than unity are not excited for a linear model, only the cases of $k=-1$, $k=0$, and $k=1$ need to be considered.

Substituting ω expression into Eqs. (20b) and (20c) leads to:

$$Re\left\{\sqrt{\frac{\alpha}{\beta}}\sum_{k=-\infty}^{\infty}A_{k}\left[\frac{C_{d}v_{\theta g}}{K}-q_{k}\right]e^{ik\theta}\right\}=0 \tag{23a}$$

$$Im\left\{\sum_{k=-\infty}^{\infty} A_k\left[\frac{2C_d v_{\theta g}}{K} - q_k\right]e^{ik\theta} + i\frac{C_d {v_{\theta g}}^2}{K}\right\} = 0 \tag{23b}$$

After a series of manipulations, one could obtain the frictional velocity components u' and v' (see detailed derivation in Appendix A). Fig. 2 presents a step-by-step procedure in the development of solutions for the proposed wind field model, where X_1, X_2, X_3, X_4 and η are five parameters defined, respectively, as follows:

$$X_1 = \left[q_0 + \frac{fr}{K}C_d - \frac{2\eta C_d}{K} - \frac{c^2 {C_d}^2}{4K^2\left(q_1 - {q_{-1}}^*\right)} + \frac{c^2 {C_d}^2}{4K^2\left({q_1}^* - q_{-1}\right)}\right] \tag{24a}$$

$$X_2 = \left[-{q_0}^* - \frac{fr}{K}C_d + \frac{2\eta C_d}{K} - \frac{c^2 {C_d}^2}{4K^2\left(q_1 - {q_{-1}}^*\right)} + \frac{c^2 {C_d}^2}{4K^2\left({q_1}^* - q_{-1}\right)}\right] \tag{24b}$$

$$X_3 = -2\frac{iC_d}{K}\left(\eta - \frac{fr}{2}\right)^2 \tag{24c}$$

$$X_4 = -\left[-q_0 - \frac{fr}{2K}C_d + \frac{\eta C_d}{K}\right] \Big/ \left[-{q_0}^* - \frac{fr}{2K}C_d + \frac{\eta C_d}{K}\right] \tag{24d}$$

$$\eta = \left[\frac{\left(-c\sin\left(\theta - \upsilon\right) - fr\right)^2}{4} + \frac{r}{\rho}\frac{\partial p}{\partial r}\right]^{1/2} \tag{24e}$$

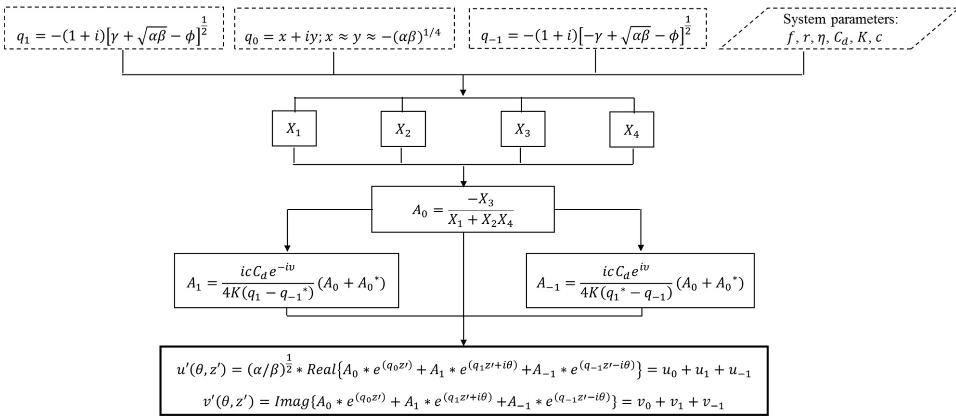

Fig. 2. u' and v' components of wind field model

As it can be seen from Fig. 2, $u'(\theta, z')$ and $v'(\theta, z')$ were decomposed respectively into three components, i.e., $u'(\theta, z') = u_0 + u_1 + u_{-1}$ and $v'(\theta, z') = v_0 + v_1 + v_{-1}$. These components (i.e., u_0, v_0, u_1, v_1, u_{-1}, v_{-1}) determine the direction and amplitude of the resultant frictional velocity. While the real and imaginary components of q_0 are approximated as: $x \approx y \approx -(\alpha\beta)^{1/4}$ as indicated in Fig. 2, their exact solutions could be obtained based on Eqs. (A.19) and (A.20) (See Appendix A for detailed derivation). The investigation of each component (i.e., u_0, v_0, u_1, v_1, u_{-1}, v_{-1}) will be discussed in section 4.1.

4. Improved Representation

In this section, the spatial distribution of wind in the tropical cyclone boundary layer will be investigated first based on a case study. Then two wind field models previously discussed by researchers, namely Kepert's model (2001) and Meng's model (1995), will be explored to demonstrate the advantages of the proposed linear height-resolving model in this study.

4.1 Spatial Distribution of the tropical cyclone wind field

To investigate the tropical cyclone spatial distribution, a case study is analyzed using the following parameters: $\Delta p = 60\,hpa$; $r_m = 80\,km$; $c = 15\ m/s$; $\upsilon = 90°C$; Latitude $\psi = 32.8°$; Longitude $\lambda = 129.7°$; $B = 1$; $z_0 = 0.1\,m$; $K = 100\ m^2/s$; and $\rho = 1.2\,N s^2/m^4$.

Figures (3a) and (3b) depict the contours of the gradient wind velocity and its three-dimensional shaded surface, respectively. It can be concluded that the maximum wind speed is located at r_m and the difference of the maximum wind velocity between the right-hand side and left-hand side is almost equal to the translational hurricane velocity *c*. Figures (3c) and (3d) illustrate the contours of the surface wind velocity at the height around 10 m and its three-dimensional shaded surface, respectively. The maximum wind speed is located on the right rear quadrant for this specific case. The exact location of the maximum wind speed depends on a number of factors such as the translation of the storm and the surface friction. Recently, Li and Hong (2014) inspected the location of the maximum wind speed based on the H*Wind data where totally 489 snapshots from 45 hurricanes, occurred during 2002 to 2013 were utilized. The H*Wind was essentially developed by the Hurricane Research Division of the National Oceanic and Atmospheric Administration (NOAA). It integrates several sources of wind data such as aircraft reconnaissance, buoys, surface and remote sensing observations (Powell et al. 1998). To ensure quality control, collected data are post-processed. The H*Wind database provides maximum 1-min sustained surface wind speed corresponding to a marine or open terrain over land exposure~~s~~. It is found that the maximum wind speed for 84% of the snapshots was located on the right side of the storm motion. More specifically, 58% of these snapshots present the maximum wind speed at the right rear quadrant and 42% at the right front quadrant.

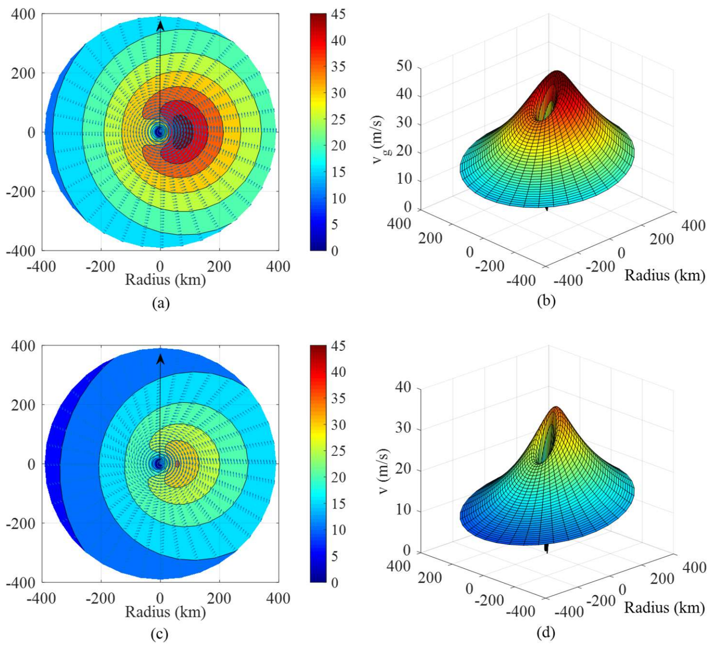

Fig. 3. Spatial distribution of the wind speed: (a) Contour of the gradient wind speed; (b) three-dimensional shaded surface of the gradient wind speed; (c) Contour of the surface wind speed at z around 10m; (d) three-dimensional shaded surface of the surface wind speed

Figure (4) shows the u_0, v_0, u_1, v_1, u_{-1}, and v_{-1} terms in the frictional component of the boundary layer wind velocity using the same tropical cyclone data as in Fig. (3). Several conclusions related to the behavior of u_0, v_0, u_1, v_1, u_{-1}, and v_{-1} terms, can be drawn. First, it is obvious that all frictional velocity components decay with height. Second, while u_1 and v_1 rotate counterclockwise u_{-1} and v_{-1} rotate clockwise. This behavior can be attributed to the signs of the imaginary parts related to z' and θ in the complex exponential argument (i.e., $e^{(q_1 z' + i\theta)}$ and $e^{(q_{-1} z' - i\theta)}$) where opposite signs results in a counterclockwise rotation and vise-versa. Finally, due to the asymmetry of the tropical cyclone wind field, the proposed model allows the vertical length scale for the depth of the boundary layer to exhibit not only radial variation but azimuthal one as well, which is not the case for Kepert's model (2001) where it varies only radially. The depth scale related to (u_0, v_0), (u_1, v_1) and (u_{-1}, v_{-1}) are $\delta_0 = 1\big/(\alpha\beta)^{\frac{1}{4}}$, $\delta_1 = 1\big/\left[\gamma + \sqrt{\alpha\beta} - \phi\right]^{\frac{1}{2}}$ and $\delta_{-1} = 1\big/\left[-\gamma + \sqrt{\alpha\beta} - \phi\right]^{\frac{1}{2}}$, respectively. For instance, δ_0 is a function of α and β which are proportional to the absolute angular velocity and vertical component of absolute vorticity of the gradient wind, respectively ($\alpha = \frac{1}{2K}\xi_g$ and $\beta = \frac{1}{2K}\xi_{ag}$). These two variables are varying radially and azimuthally due to the asymmetric structure of a moving tropical cyclone, therefore δ_0 exhibits an asymmetric distribution. Since the rotational rate of each frictional component with height is dependent on the corresponding depth scale, it can be concluded from the comparison of δ_1 and δ_{-1} that (u_1, v_1) rotates faster than (u_{-1}, v_{-1}), as indicated in the simulation results of Fig. 4.

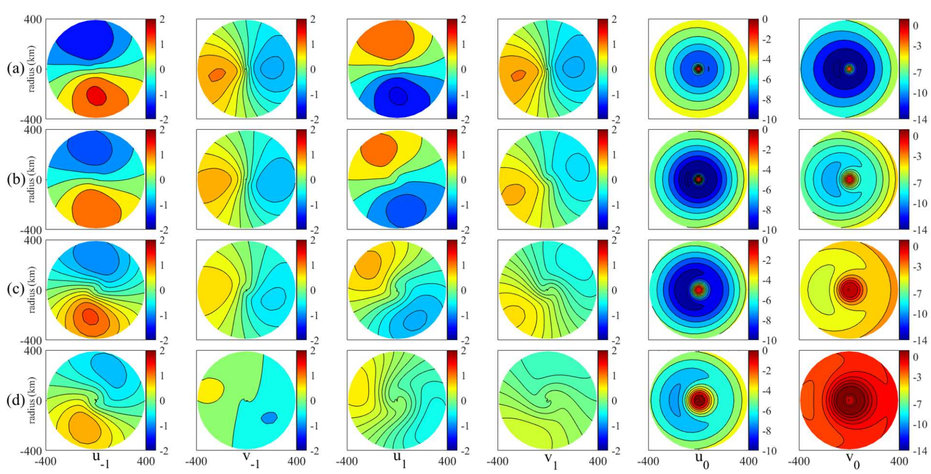

Fig. 4. Frictional component of the boundary layer wind velocity u_0, v_0, u_1, v_1, u_{-1}, and v_{-1} at z'=10m (a); z'=200m (b); z'=500m (c); and z'=1000m (d)

Figure 5 depicts the radial variation of the three depth scales δ_0, δ_1, δ_{-1}. It can be concluded that for larger radii all depth scales reduce to the classical Ekman height scale (namely $\delta = \sqrt{2K/f}$), where the Rossby number that measures the magnitude of the acceleration compared to the Coriolis force is sufficiently small $(Ro \ll 1)$ ~~$(Ro$□$1)$~~. On the other hand, the boundary layer depth decreases toward the center of the tropical cyclone (large Rossby numbers) due to the effects of the storm rotation that results in predominated inertial and centrifugal forces, as highlighted by several researchers (e.g., Rosenthal 1962; Kepert 2001). The results shown in Fig. 5 are consistent with several numerical simulations and observations conducted by several researchers (e.g., Kepert 2001; Kepert and Wang 2001) where the boundary layer depth varies from a few hundred meters near from the inner core of the tropical cyclone to 1-3 km at larger radii. Table 4 depicts the azimuthal variation of the depth scale for all frictional components. Clearly, all depth scales depend on the azimuthal coordinate and thus should be taken into consideration to enhance the simulation of the real behavior of a moving tropical cyclone.

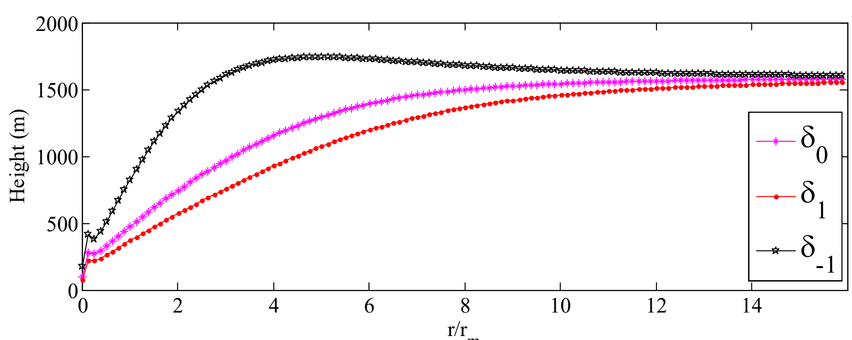

Fig. 5. Radial variation of the depth scale of the boundary layer

Table 4. Boundary layer depth scale at $r = r_m$ (using the same tropical cyclone data of section 4.1)

$\theta(°)$	$\delta_0(m)$	$\delta_1(m)$	$\delta_{-1}(m)$
0	477.2	369.7	826.0
30	482.3	367.4	769.2
60	496.4	374.1	749.0
90	516.2	388.1	761.5
120	536.3	406.0	800.6
150	551.3	423.1	858.9
180	556.7	434.6	929.1
210	551.3	437.4	1002.7
240	536.3	430.6	1062.0
270	516.2	415.9	1073.7
300	496.4	397.4	1015.0
330	482.3	380.4	916.0
360	477.2	369.7	826.0

4.2 Stationary tropical cyclone

For a stationary tropical cyclone, the translational velocity $c = 0$, and hence $A_1 = A_{-1} = 0$. Accordingly, the frictional wind velocity components are degenerated into $u'(\theta, z') = (\alpha/\beta)^{\frac{1}{2}} * Real\{A_0 * \exp(q_0 z')\}$ and $v'(\theta, z') = Imag\{A_0 * \exp(q_0 z')\}$ with $q_0 = -(1+i)(\alpha\beta)^{1/4}$. It can be demonstrated in the stationary case that:

$$X_1 = -(\alpha\beta)^{\frac{1}{4}}(1+i) - \frac{2C_D}{K} v_g \tag{25a}$$

$$X_2 = (\alpha\beta)^{\frac{1}{4}}(1-i) + \frac{2C_D}{K} v_g \tag{25b}$$

$$X_3 = -\frac{2iC_D}{K} v_g^{\ 2} \tag{25c}$$

$$X_4 = -\left[(\alpha\beta)^{\frac{1}{4}}(1+i) + \frac{C_D}{K} v_g\right] \Big/ \left[(\alpha\beta)^{\frac{1}{4}}(1-i) + \frac{C_D}{K} v_g\right] \tag{25d}$$

It should be noted that $v_{\theta g}$ was replaced by v_g since the gradient wind is symmetric for a stationary tropical cyclone. In Kepert (2001) a parameter X is defined as $C_D v_g \big/ K(\alpha\beta)^{\frac{1}{4}}$. Then A_0 of a stationary tropical cyclone could be expressed in terms of X as:

$$A_0 = -\frac{X\left[1+i(1+X)\right]v_g}{2X^2+3X+2} \tag{26}$$

The expression is exactly the same with that of Kepert (2001). This indicates that the specific case of the stationary tropical cyclone in the proposed model provides the same solution in Kepert (2001). This observation is expected since the gradient wind velocity for the case of a stationary tropical cyclone is symmetric, which was an essential assumption in Kepert (2001).

4.3 Comparison with Meng's model

The wind field model in Meng et al. (1995) is a special case of the present study. More specifically, the contribution associated with u_1, u_{-1}, v_1, v_{-1} and ϕ was disregarded by Meng et al. (1995). Accordingly, suppose $u_1 = u_{-1} = v_1 = v_{-1} = \phi = 0$, one has (see Appendix B for detailed derivation):

$$u(\theta, z') = -(\alpha/\beta)^{\frac{1}{2}} e^{-\lambda z'} \left[\frac{\chi v_{\theta g}}{1+(1+\chi)^2}\cos(\lambda z') + \frac{\chi(\chi+1)v_{\theta g}}{1+(1+\chi)^2}\sin(\lambda z') \right] \tag{27a}$$

$$v(\theta, z') = e^{-\lambda z'} \left[-\frac{\chi(\chi+1)v_{\theta g}}{1+(1+\chi)^2}\cos(\lambda z') + \frac{\chi v_{\theta g}}{1+(1+\chi)^2}\sin(\lambda z') \right] \tag{27b}$$

where $\chi = \frac{C_d}{K\lambda}|v_s| = \frac{C_d}{K\lambda}\sqrt{{v_{\theta s}}^2 + {v_{rs}}^2}$

The solution developed by Meng et al. (1995) has similar form:

$$u = -\xi e^{-\lambda z'} * \left[D_2 \cos(\lambda z') - D_1 \sin(\lambda z') \right] \tag{28a}$$

$$v = e^{(-\lambda z')} * [D_1 \cos(\lambda z') + D_2 \sin(\lambda z')] \tag{28b}$$

where $D_1 = -\chi(\chi+1)v_{\theta g} \big/ 1+(1+\chi)^2$; $D_2 = \chi v_{\theta g} \big/ 1+(1+\chi)^2$; and $\xi = (\beta/\alpha)^{\frac{1}{2}}$. Consequently, it is shown that Meng's model (1995) can be derived from the proposed model under the above-mentioned assumptions. By comparison between Eqs. (27a) and (28a), it is noted that there is an error in Meng's original model, where the coefficient ξ should be replaced by $1/\xi$. This modification of the wind speed due to this error may not be negligible, as will be illustrated in the validation example.

5. Validation

To validate the new tropical cyclone wind field model, wind records from hurricane Fran (1996) and typhoon Maemi T0314 (2003) are used.

5.1 Hurricane Fran

Fran was one of the worst hurricanes ever to be recorded in North Carolina. It ~~has~~ reached hurricane status on ~~29th~~ August 29th, 1996 and was registered as a Category 3 storm. Hurricane Fran made landfall on September 5th~~, 1996~~ on the North Carolina coast with an estimated central pressure of $954\,hpa$ ~~and a maximum sustained surface winds of $50\,m/s$~~. It created flooding in the Carolinas, Virginia, West Virginia and Pennsylvania. Severe damage due to strong wind were also recorded. Fran weakened to a tropical storm status over central North Carolina. Figure 6 depicts the location of the anemometer with respect to the storm track.

Mis en forme : Exposant

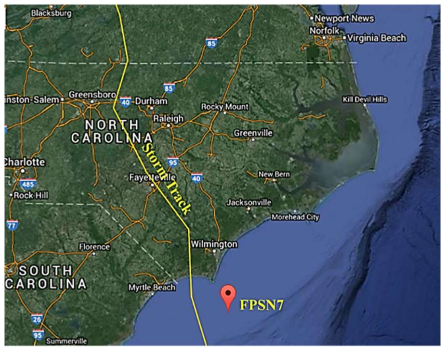

Fig. 6. Track of hurricane Fran and anemometer location

5.1.1 Hurricane Parameters

The necessary parameters for the simulation were recorded by the marine station FPSN7 from September 5^{th} to September 6^{th}. The station ID is 41013, located at (N33.44°,W77.74°). The National Hurricane Center's North Atlantic hurricane database (HURDAT) (Jarvinen et al. 1984) is the primary source of data. Typically, the parameters needed for the simulation are: υ approach angle; c translation velocity of the hurricane; p_c central pressure; Δp central pressure difference; r_m radius of maximum winds; ψ latitude; and λ longitude. The parameter r_m can be estimated using several sources in the literature (e.g., Powell et al. 1991; 1998). This information is supplemented by the H*Wind snapshots. There are several methods available in the literature to estimate the parameter B (e.g., Vickery et al. 2000a; Holland 2008). For hurricane Fran the value used was $B = 0.95$, which is the same value calculated by Vickery et al. (2000b). The period from September 5^{th} to September 6^{th} has known very strong winds from hurricane Fran especially in the eyewall region. Actually, the central pressure reached 952 hpa at 0600 UTC September 5^{th} in which the hurricane center was located at (N29.8°,W76.7°) and slightly increased to reach

954 hpa at 0000 UTC September 6th where the hurricane center was located at (N33.7°,W78.0°) with a maximum sustained surface winds of 55 m/s.

5.1.2 Hurricane Simulation

The observed wind speeds and directions have been compared with those obtained by the proposed wind field model. It should be noted that all parameters are obtained from the 6-hour interval track information provided by the HURDAT database. The results generated by the present model are consistent with hurricane observations as depicted in the Fig. 7.

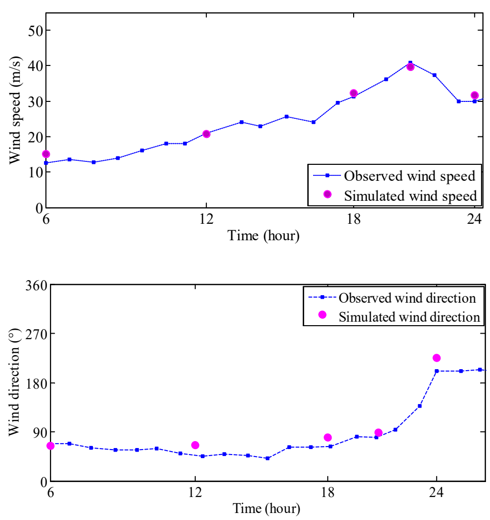

Fig. 7. Observed and simulated wind speeds (top) and directions (bottom) of Hurricane Fran

5.2 Typhoon Maemi

Typhoon Maemi T0314 had devastating impacts on Japan and South Korea. It was born as tropical depression near Guam on September 5th, 2003. Later, it was evolved into a typhoon on ~~the~~ September 7th ~~of September~~ and then intensified to reach a Category 5 typhoon storm ~~reaching~~ with a central pressure of 910 hpa. Maemi made landfall on September 12~~, 2003~~ on the south coast of the Korean peninsula and lasted approximately 6 hours in the South Korea leading to extensive damage from wind, torrential rainfall and flooding. Wind records from typhoon Maemi will be employed to highlight the difference between the results generated by the present model and Meng's model.

5.2.1 Typhoon Parameters

The observation point is located at the observatory of Miyako Island in Okinawa prefecture (N24.8°, E125.3°). All the other necessary parameters for the typhoon simulation are obtained from Yoshida et al. (2008), and listed in Table 5 for completeness:

Table 5. Typhoon Maemi parameters, September 2003 (Yoshida et al., 2008)

Day/h	$\psi(°)$	$\lambda(°)$	$\upsilon(°)$	$c(m/s)$	$p_c(hPa)$	$\Delta p(hPa)$	$r_m(km)$
10|12	23.7	126.9	143.8	3.29	920	88	23.2
10|18	24.2	126.3	118.6	2.99	910	99	29.5
11|00	24.6	125.7	75.6	3.29	910	100	34.7
11|06	24.8	125.3	76.2	2.88	910	101	31.0
11|12	25.7	125.3	78.5	3.70	923	89	40.7
11|18	27.0	125.5	75.1	5.79	930	82	42.9
12|00	28.7	125.9	71.6	7.25	935	77	43.3

5.2.2 Typhoon Simulation

The observed wind speeds and directions have been compared with those obtained by the proposed wind field model. In addition, simulation results of the original and modified Meng's models are presented. As shown in Fig. 8, the results generated by the present model are consistent with the typhoon observations.

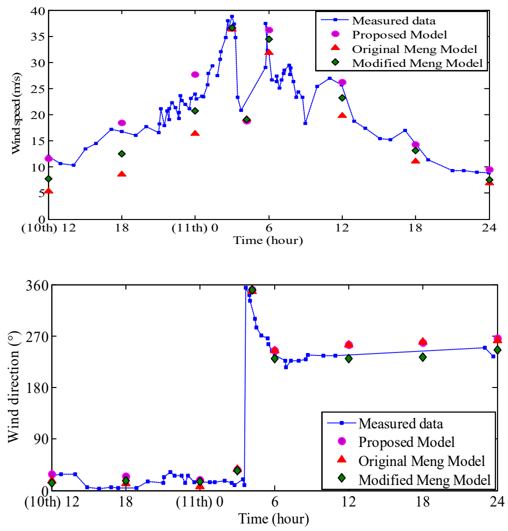

Fig. 8. Observed and simulated wind speeds (top) and directions (bottom) of typhoon Maemi

To further inspect the results, a comparison of wind speeds and directions between results obtained from the observed data and using the present and Meng's models are presented in Fig. 9. The corresponding correlation coefficients between the observations and various simulations for wind speed and direction are calculated and presented in Table 6.

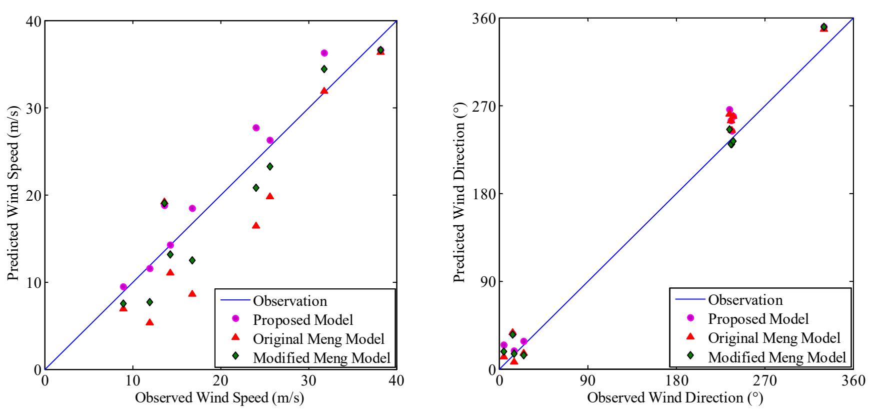

Fig. 9. Comparison of wind speeds (left) and directions (right)

Table 6. Correlation Coefficients of wind speed and direction

Model	Wind speed	Wind direction
Proposed Model	0.973	0.998
Meng's model (original)	0.916	0.997
Meng's model (modified)	0.953	0.995

The results demonstrate that the wind velocities predicted by various models all match reasonably well with the measured data, whereas the proposed model is superior to Meng's model.

5.3 Vertical wind speed profile

Vertical wind speed profiles given by the proposed model, original and modified Meng's models, are plotted in Fig. 10 using the same tropical data of section 4.1. The location of the presented wind speed profiles is selected at a distance equal to radius of maximum wind from the tropical cyclone center and at zero degree from the East. The simulated wind profiles are normalized by the gradient wind speed.

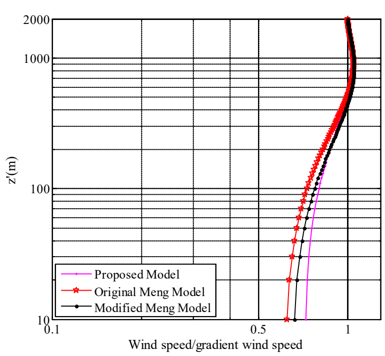

Fig. 10. Vertical profile of wind speed at $r = r_m$

As it can be remarked from Fig. 10, the surface wind speed is underestimated by Meng's model compared to the proposed one. Same conclusion could be also obtained from the simulation results in Fig. 8. Another interesting feature in the vertical wind speed profile of tropical cyclones is the presence of a super-gradient-wind region, where the tangential winds are larger than the gradient wind. A possible mechanism of this region was discussed by Kepert and Wang (2001), where the super-gradient winds are attributed to the strong inward advection of angular momentum. It is important to take the super-gradient wind region into account in the engineering applications such as the wind design of high-rise buildings to ensure the target safety and performance levels of civil infrastructures. As a result, the power or logarithmic law profiles and hence the use of reduction factors to obtain the surface winds may not be appropriate for many structures in the coastal regions.

6. Concluding Remarks

A linear height-resolving analytical model for the boundary layer winds of a translating tropical cyclone has been developed and validated in this study. The construction of the new model started from the Navier-Stokes equations coupled with the decomposition method. The obtained dynamic system was then simplified based on the scale analysis. Finally, a simple height-resolving solution of the wind field was analytically obtained by linearization techniques with the imposed boundary conditions at upper atmosphere and above ground surface. The general solution for a stationary tropical cyclone was found to be consistent with the one discussed by Kepert (2001). Also, it is demonstrated that Meng et al. (1995) model is a special case of the present solution for the wind field in tropical cyclones. Furthermore, it was demonstrated that the vertical length scale for the depth of the boundary layer related to each component of the frictional wind velocity exhibited not only radial variation but azimuthal one as well, which is conform to the asymmetric structure of a moving tropical cyclone. The present model shows great promise in giving a first-order approximation of the boundary layer wind field of a tropical cyclone. Due to its simplicity and computational efficiency, the proposed wind field model could be easily implemented in the risk assessments of engineering applications.

APPENDIX A

To solve Eqs. (23a) and (23b), the gradient wind which depends on the radial and azimuthal coordinates, is expanded with respect to θ. Accordingly, $v_{\theta g}$ could be expressed as:

$$v_{\theta g} = \frac{\left(-c\sin\left(\theta-\upsilon\right)-fr\right)}{2} + \left[\frac{\left(-c\sin\left(\theta-\upsilon\right)-fr\right)^2}{4} + \frac{r}{\rho}\frac{\partial p}{\partial r}\right]^{1/2} = \tau+\eta \qquad \text{(A.1)}$$

It is shown that the η term is much less sensitive to the azimuthal coordinate compared to the term τ, as numerically verified in Table A.1.

Table A.1 Comparison of η and τ (using the same tropical cyclone data of section 4.1)

$\theta(°)$	$r = r_m$		$r = 2r_m$	
	$\tau(m/s)$	$\eta(m/s)$	$\tau(m/s)$	$\eta(m/s)$
0	4.34	43.11	1.18	38.96
30	3.33	43.01	0.17	38.94
60	0.59	42.89	-2.57	39.02
90	-3.16	43.00	-6.32	39.35
120	-6.91	43.44	-10.07	40.22
180	-10.66	44.19	-13.82	41.32
270	-3.16	43.00	-6.32	39.45

Substituting Eq. (A.1) into Eqs. (23a) and (23b), where η is treated azimuthal coordinate independent, yields:

$$Re\left\{\sqrt{\frac{\alpha}{\beta}}\sum_{k=-\infty}^{\infty}A_k\left[\frac{C_d}{K}\left(\frac{ic}{4}\left(e^{i(\theta-\upsilon)}-e^{-i(\theta-\upsilon)}\right)-\frac{fr}{2}+\eta\right)-q_k\right]e^{ik\theta}\right\}=0 \qquad \text{(A.2)}$$

$$Im\left\{\sum_{k=-\infty}^{\infty} A_k\left[\frac{2C_d}{K}\left(\frac{ic}{4}\left(e^{i(\theta-\upsilon)}-e^{-i(\theta-\upsilon)}\right)-\frac{fr}{2}+\eta\right)-q_k\right]e^{ik\theta}+i\frac{C_d}{K}\left(\frac{ic}{4}\left(e^{i(\theta-\upsilon)}-e^{-i(\theta-\upsilon)}\right)-\frac{fr}{2}+\eta\right)^2\right\}=0 \tag{A.3}$$

After several algebraic manipulations, one can obtain:

$$\left[-q_0-\frac{fr}{2K}C_d+\frac{\eta C_d}{K}\right]A_0+\left[-q_0^*-\frac{fr}{2K}C_d+\frac{\eta C_d}{K}\right]A_0^*=0 \tag{A.4}$$

$$A_1+A_{-1}^*=0 \tag{A.5}$$

$$\frac{iC_d c}{4K}e^{-i\upsilon}A_0+\frac{iC_d c}{4K}e^{-i\upsilon}A_0^*+\left(-q_1+q_{-1}^*\right)A_1=0 \tag{A.6}$$

$$\begin{aligned}\left[q_0+\frac{fr}{K}C_d-\frac{2\eta C_d}{K}\right]A_0+\left[-q_0^*-\frac{fr}{K}C_d+\frac{2\eta C_d}{K}\right]A_0^*+\frac{icC_d}{K}e^{i\upsilon}A_1\\ -\frac{icC_d}{K}e^{-i\upsilon}A_{-1}-2\frac{iC_d}{K}\left(\eta-\frac{fr}{2}\right)^2=0\end{aligned} \tag{A.7}$$

Based on Eq. (A.5), q_1 and q_{-1} could be derived from Eq. (22), hence:

$$q_1=-\left(1+i\right)\left[\gamma+\sqrt{\alpha\beta}-\phi\right]^{\frac{1}{2}} \tag{A.8}$$

$$q_{-1}=-\left(1+i\right)\left[-\gamma+\sqrt{\alpha\beta}-\phi\right]^{\frac{1}{2}} \tag{A.9}$$

A_1 and A_{-1} expressions could be derived from Eqs. (A.5) and (A.6), hence:

$$A_1=\frac{icC_d e^{-i\upsilon}}{4K\left(q_1-q_{-1}^*\right)}\left(A_0+A_0^*\right) \tag{A.10}$$

$$A_{-1}=-A_1^*=\frac{icC_d e^{i\upsilon}}{4K\left(q_1^*-q_{-1}\right)}\left(A_0+A_0^*\right) \tag{A.11}$$

Substituting Eqs. (A.10) and (A.11) into Eq. (A.7) gives:

$$X_1A_0+X_2A_0^*+X_3=0 \tag{A.12}$$

where X_1, X_2, and X_3 are expressed as follows:

$$X_1 = \left[q_0 + \frac{fr}{K} C_d - \frac{2\eta C_d}{K} - \frac{c^2 C_d^{\,2}}{4K^2 \left(q_1 - q_{-1}^{\;*} \right)} + \frac{c^2 C_d^{\,2}}{4K^2 \left(q_1^{\,*} - q_{-1} \right)} \right] \tag{A.13}$$

$$X_2 = \left[-q_0^{\,*} - \frac{fr}{K} C_d + \frac{2\eta C_d}{K} - \frac{c^2 C_d^{\,2}}{4K^2 \left(q_1 - q_{-1}^{\;*} \right)} + \frac{c^2 C_d^{\,2}}{4K^2 \left(q_1^{\,*} - q_{-1} \right)} \right] \tag{A.14}$$

$$X_3 = -2 \frac{iC_d}{K} \left(\eta - \frac{fr}{2} \right)^2 \tag{A.15}$$

On the other hand Eq. (A.4) could be expressed as:

$$A_0^{\,*} = X_4 \, A_0 \tag{A.16}$$

where X_4 is:

$$X_4 = -\left[-q_0 - \frac{fr}{2K} C_d + \frac{\eta C_d}{K} \right] \Big/ \left[-q_0^{\,*} - \frac{fr}{2K} C_d + \frac{\eta C_d}{K} \right] \tag{A.17}$$

As a result, the following equation could be obtained:

$$q_0^{\,2} \left[\left(\eta - \frac{fr}{2} \right) \frac{C_d}{K} - q_0^{\,*} \right] = i \left[2\sqrt{\alpha\beta} - \phi \right] \left[\left(\eta - \frac{fr}{2} \right) \frac{C_d}{K} - q_0^{\,*} \right] - i\phi \left[\left(\eta - \frac{fr}{2} \right) \frac{C_d}{K} - q_0 \right] \tag{A.18}$$

To determine q_0, it could be expressed in the complex form as $q_0 = x + iy$ where $x < 0$ to be consistent with the boundary condition of Eq. (15a). Hence, the following system of equations is obtained:

$$-x^3 + \left(\eta - \frac{fr}{2} \right) \frac{C_d}{K} x^2 - xy^2 - \left(\eta - \frac{fr}{2} \right) \frac{C_d}{K} y^2 + 2\sqrt{\alpha\beta}\, y = 0 \tag{A.19}$$

$$-x^2 y + 2\left(\eta - \frac{fr}{2} \right) \frac{C_d}{K} xy + \left(2\sqrt{\alpha\beta} - 2\phi \right) x - y^3 + \left(-2\sqrt{\alpha\beta} + 2\phi \right) \left(\eta - \frac{fr}{2} \right) \frac{C_d}{K} = 0 \tag{A.20}$$

Consider a stationary tropical cyclone where $\phi = 0$, one has:

$$x = y \approx -\left(\alpha\beta \right)^{1/4} \tag{A.21}$$

Substituting the above-mentioned approximation into Eqs. (A.19) and (A.20) results in a required condition of $\phi(\alpha\beta)^{1/4}+\phi\left(\eta-\frac{fr}{2}\right)\frac{C_d}{K}=0$. Using the data of section 4.1 corresponding to a typical tropical cyclone, the value of $\phi(\alpha\beta)^{1/4}+\phi\left(\eta-\frac{fr}{2}\right)\frac{C_d}{K}$ is approximately 10^{-9}. Hence, it is suggested that $x=y\approx-(\alpha\beta)^{1/4}$ could be adopted for any typical tropical cyclone.

On the other hand A_0 can be determined from Eqs. (A.12) and (A.16):

$$A_0=\frac{-X_3}{X_1+X_2X_4} \tag{A.22}$$

Hence the frictional components of the wind velocity are:

$$u'(\theta,z')=\left(\frac{\alpha}{\beta}\right)^{\frac{1}{2}}*Real(\omega)=\left(\frac{\alpha}{\beta}\right)^{\frac{1}{2}}*Real\left\{A_0*e^{(q_0z')}+A_1*e^{(q_1z'+i\theta)}+A_{-1}*e^{(q_{-1}z'-i\theta)}\right\}=u_0+u_1+u_{-1} \tag{A.23}$$

$$v'(\theta,z')=Imag(\omega)=Imag\{A_0*e^{(q_0z')}+A_1*e^{(q_1z'+i\theta)}+A_{-1}*e^{(q_{-1}z'-i\theta)}\}=v_0+v_1+v_{-1} \tag{A.24}$$

APPENDIX B

To obtain the solution of the proposed model in the case $u_1=u_{-1}=v_1=v_{-1}=\phi=0$, the A_0 can be expressed in the complex form as a_1+ia_2. In addition, the expression of q_0 could be derived from Eq. (22):

$$q_0=\left[2i\sqrt{\alpha\beta}\right]^{1/2}=-\lambda(1+i) \tag{B.1}$$

where $\lambda=(\alpha\beta)^{\frac{1}{4}}$. As a result, the frictional components of the wind velocity can be explicitly given as:

$$u'(\theta,z') = \left(\frac{\alpha}{\beta}\right)^{\frac{1}{2}} * Real\left\{A_0 * \exp\left(q_0 z'\right)\right\} = \left(\frac{\alpha}{\beta}\right)^{\frac{1}{2}} e^{-\lambda z'} * \left[a_1 \cos\left(-\lambda z'\right) - a_2 \sin\left(-\lambda z'\right)\right] \tag{B.2}$$

$$v'(\theta,z') = Imag\{A_0 * \exp\left(q_0 z'\right)\} = e^{-\lambda z'} * \left[a_2 \cos\left(-\lambda z'\right) + a_1 \sin\left(-\lambda z'\right)\right] \tag{B.3}$$

According to the relationship $A_0 q_0 = \left.\frac{\partial \omega}{\partial z}\right|_{z'=0}$, A_0 can be determined as:

$$A_0 = \frac{1}{q_0}\left.\frac{\partial \omega}{\partial z}\right|_{z'=0} = \frac{1}{q_0}\left[\sqrt{\frac{\beta}{\alpha}}\left.\frac{\partial u'}{\partial z}\right|_{z'=0} + i\left.\frac{\partial v'}{\partial z}\right|_{z'=0}\right] \tag{B.4}$$

The ground surface wind velocity components can be denoted as: $v_{rs} = u_0' = \sqrt{\alpha/\beta}\, a_1$ and $v_{\theta s} = v_0' + v_{\theta g} = a_2 + v_{\theta g}$ where $a_1 + i a_2 = \omega\left(z=0\right) = \sqrt{\beta/\alpha}\, u_0' + i v_0'$. Based on Eq. (15b) and substituting the expressions of $\left.\frac{\partial u'}{\partial z}\right|_{z'=0}$ and $\left.\frac{\partial v'}{\partial z}\right|_{z'=0}$ into Eq. (B.4), results in:

$$a_1 - a_2 = -\sqrt{\frac{\beta}{\alpha}}\chi v_{rs} = -\chi a_1 \tag{B.5}$$

$$a_1 + a_2 = -\chi v_{\theta s} = -\chi\left(a_2 + v_{\theta g}\right) \tag{B.6}$$

where $\chi = \frac{C_d}{K\lambda}\left|v_s\right| = \frac{C_d}{K\lambda}\sqrt{{v_{\theta s}}^2 + {v_{rs}}^2}$. Solving Eqs. (B.5) and (B.6) leads to the following results:

$$a_1 = -\frac{\chi v_{\theta g}}{1 + \left(1 + \chi\right)^2} \tag{B.7}$$

$$a_2 = -\frac{\chi\left(\chi + 1\right) v_{\theta g}}{1 + \left(1 + \chi\right)^2} \tag{B.8}$$

Hence, one obtains the frictional components of the wind velocity as:

$$u'(\theta,z') = -\left(\frac{\alpha}{\beta}\right)^{\frac{1}{2}} e^{-\lambda z'} * \left[\frac{\chi v_{\theta g}}{1 + \left(1 + \chi\right)^2}\cos\left(\lambda z'\right) + \frac{\chi\left(\chi + 1\right) v_{\theta g}}{1 + \left(1 + \chi\right)^2}\sin\left(\lambda z'\right)\right] \tag{B.9}$$

$$v'(\theta,z') = e^{-\lambda z'} * \left[-\frac{\chi(\chi+1)v_{\theta g}}{1+(1+\chi)^2}\cos(\lambda z') + \frac{\chi v_{\theta g}}{1+(1+\chi)^2}\sin(\lambda z') \right] \tag{B.10}$$

Acknowledgements

The support for this project provided by the NSF Grant # CMMI 15-37431 is gratefully acknowledged.

References

Carrier, G.F., Hammond, A.L. and George, O.D., 1971. A model of the mature hurricane. Journal of Fluid Mechanics, 47(1), pp.145-170.

Chow, S.H., 1971. A study of the wind field in the planetary boundary layer of a moving tropical cyclone (Master Thesis, New York University, New York, USA).

Georgiou, P.N., 1986. Design wind speeds in tropical cyclone-prone regions (PhD Thesis, University of Western Ontario, London, Ontario, Canada).

Haurwitz, B., 1935. The height of tropical cyclones and the" eye" of the storm. Monthly Weather Review, 63, pp.45–49.

Haurwitz, B., 1936. On the structure of tropical cyclones. Quarterly Journal of the Royal Meteorological Society, 62(263), pp.145-146.

Holland, G.J., 1980. An analytic model of the wind and pressure profiles in hurricanes. Monthly weather review, 108(8), pp.1212-1218.

Holland, G., 2008. A revised hurricane pressure–wind model. Monthly Weather Review, 136(9), pp.3432-3445.

Hubbert, G.D., Holland, G.J., Leslie, L.M. and Manton, M.J., 1991. A real-time system for forecasting tropical cyclone storm surges. Weather and Forecasting, 6(1), pp.86-97.

Jarvinen, B.R., Neumann, C.J. and Davis, M.A.S., 1984. A tropical cyclone data tape for the North Atlantic Basin, 1886–1983: Contents, limitations, and uses. Tech. Memo. NWS NHC 22, National Oceanic and Atmospheric Administration.

Kennedy, A.B., Westerink, J.J., Smith, J.M., Hope, M.E., Hartman, M., Taflanidis, A.A., Tanaka, S., Westerink, H., Cheung, K.F., Smith, T. and Hamann, M., 2012. Tropical cyclone inundation potential on the Hawaiian Islands of Oahu and Kauai. Ocean Modelling, 52, pp.54-68.

Kepert, J., 2001. The dynamics of boundary layer jets within the tropical cyclone core. Part I: Linear theory. Journal of the Atmospheric Sciences, 58(17), pp.2469-2484.

Kepert, J. and Wang, Y., 2001. The dynamics of boundary layer jets within the tropical cyclone core. Part II: Nonlinear enhancement. Journal of the atmospheric sciences, 58(17), pp.2485-2501.

Kepert, J.D., 2010a. Slab-and height-resolving models of the tropical cyclone boundary layer. Part I: Comparing the simulations. Quarterly Journal of the Royal Meteorological Society, 136(652), pp.1686-1699.

Kepert, J.D., 2010b. Slab-and height-resolving models of the tropical cyclone boundary layer. Part II: Why the simulations differ. Quarterly Journal of the Royal Meteorological Society, 136(652), pp.1700-1711.

Khare, S.P., Bonazzi, A., West, N., Bellone, E. and Jewson, S., 2009. On the modelling of over-ocean hurricane surface winds and their uncertainty. Quarterly Journal of the Royal Meteorological Society, 135(642), pp.1350-1365.

Li, S.H. and Hong, H.P., 2014. Observations on a hurricane wind hazard model used to map extreme hurricane wind speed. Journal of Structural Engineering, 141(10), p.04014238.

Meng, Y., Matsui, M. and Hibi, K., 1995. An analytical model for simulation of the wind field in a typhoon boundary layer. Journal of Wind Engineering and Industrial Aerodynamics, 56(2-3), pp.291-310.

Meng, Y., Matsui, M. and Hibi, K., 1997. A numerical study of the wind field in a typhoon boundary layer. Journal of Wind Engineering and Industrial Aerodynamics, 67, pp.437-448.

Powell, M.D., Dodge, P.P. and Black, M.L., 1991. The landfall of Hurricane Hugo in the Carolinas: Surface wind distribution. Weather and forecasting, 6(3), pp.379-399.

Powell, M.D., Houston, S.H., Amat, L.R. and Morisseau-Leroy, N., 1998. The HRD real-time hurricane wind analysis system. Journal of Wind Engineering and Industrial Aerodynamics, 77, pp.53-64.

Powell, M., Soukup, G., Cocke, S., Gulati, S., Morisseau-Leroy, N., Hamid, S., Dorst, N. and Axe, L., 2005. State of Florida hurricane loss projection model: Atmospheric science component. Journal of wind engineering and industrial aerodynamics, 93(8), pp.651-674.

Rosenthal, S.L., 1962. A theoretical analysis of the field of motion in hurricane boundary layer. National Hurricane Research Project Report, (56), p.12p.

Russell, L.R., 1971. Probability distributions for hurricane effects. Journal of Waterways, Harbors & Coast Eng Div, 97(1), pp.139–154.

Schloemer, R.W., 1954. Analysis and synthesis of hurricane wind patterns over Lake Okeechobee. NOAA Hydrometeorology Report 31, Department of Commerce and U.S. Army Corps of Engineers, U.S. Weather Bureau, Washington, D.C., 49.

Shapiro, L.J., 1983. The asymmetric boundary layer flow under a translating hurricane. Journal of the Atmospheric Sciences, 40(8), pp.1984-1998.

Thompson, E.F. and Cardone, V.J., 1996. Practical modeling of hurricane surface wind fields. Journal of Waterway, Port, Coastal, and Ocean Engineering, 122(4), pp.195-205.

Vickery, P.J., Skerlj, P.F. and Twisdale, L.A., 2000a. Simulation of hurricane risk in the US using empirical track model. Journal of structural engineering, 126(10), pp.1222-1237.

Vickery, P.J., Skerlj, P.F., Steckley, A.C. and Twisdale, L.A., 2000b. Hurricane wind field model for use in hurricane simulations. Journal of Structural Engineering, 126(10), pp.1203-1221.

Vickery, P.J., Skerlj, P.F., Lin, J., Twisdale Jr, L.A., Young, M.A. and Lavelle, F.M., 2006. HAZUS-MH hurricane model methodology. II: Damage and loss estimation. Natural Hazards Review, 7(2), pp.94-103.

Vogl, S. and Smith, R.K., 2009. Limitations of a linear model for the hurricane boundary layer. Quarterly Journal of the Royal Meteorological Society, 135(641), pp.839-850.

Yoshida, M., Yamamoto, M., Takagi, K. and Ohkuma, T., 2008. Prediction of typhoon wind by Level 2.5 closure model. Journal of Wind Engineering and Industrial Aerodynamics, 96(10), pp.2104-2120.

Yoshizumi, S., 1968. On the asymmetry of wind distribution in the lower layer in typhoon. Journal of the Meteorological Society of Japan. Ser. II, 46(3), pp.153-159.